AFRL-RX-WP-JA-2020-0259

BENDING MECHANICS OF CYLINDRICAL SKINS FOR MORPHING AEROSPACE APPLICATIONS (POSTPRINT)

Jeffery W. Baur

AFRL/RXCC

Wesley A. Chapkin, David Ryan Seifert, Maria R. Ward Rashidi

United Technology Corporation

19 August 2019
Interim Report

DISTRIBUTION STATEMENT A.
Approved for public release: distribution is unlimited.

© OPEN ACCESS

(STINFO COPY)

AIR FORCE RESEARCH LABORATORY
MATERIALS AND MANUFACTURING DIRECTORATE
WRIGHT-PATTERSON AIR FORCE BASE, OH 45433-7750
AIR FORCE MATERIEL COMMAND
UNITED STATES AIR FORCE

REPORT DOCUMENTATION PAGE

Form Approved
OMB No. 0704-0188

The public reporting burden for this collection of information is estimated to average 1 hour per response, including the time for reviewing instructions, searching existing data sources, gathering and maintaining the data needed, and completing and reviewing the collection of information. Send comments regarding this burden estimate or any other aspect of this collection of information, including suggestions for reducing this burden, to Department of Defense, Washington Headquarters Services, Directorate for Information Operations and Reports (0704-0188), 1215 Jefferson Davis Highway, Suite 1204, Arlington, VA 22202-4302. Respondents should be aware that notwithstanding any other provision of law, no person shall be subject to any penalty for failing to comply with a collection of information if it does not display a currently valid OMB control number. **PLEASE DO NOT RETURN YOUR FORM TO THE ABOVE ADDRESS**.

1. REPORT DATE *(DD-MM-YY)*	2. REPORT TYPE	3. DATES COVERED *(From - To)*
19 August 2019	Interim	22 July 2013 – 19 July 2019

4. TITLE AND SUBTITLE
Bending Mechanics of Cylindrical Skins for Morphing Aerospace Applications (Postprint)

5a. CONTRACT NUMBER
In House

5b. GRANT NUMBER

5c. PROGRAM ELEMENT NUMBER

6. AUTHOR(S)
Jeffery W. Baur - AFRL/RXCC

(Continued on next page)

5d. PROJECT NUMBER

5e. TASK NUMBER

5f. WORK UNIT NUMBER
X0S7

7. PERFORMING ORGANIZATION NAME(S) AND ADDRESS(ES)
AFRL/RX
2977 Hobson Way (Continued on next page)
Wright-Patterson AFB OH 45433

8. PERFORMING ORGANIZATION REPORT NUMBER

9. SPONSORING/MONITORING AGENCY NAME(S) AND ADDRESS(ES)
Air Force Research Laboratory
Materials and Manufacturing Directorate
Wright-Patterson Air Force Base, OH 45433-7750
Air Force Materiel Command
United States Air Force

10. SPONSORING/MONITORING AGENCY ACRONYM(S)
AFRL/RXCC

11. SPONSORING/MONITORING AGENCY REPORT NUMBER(S)
AFRL-RX-WP-JA-2020-0259

12. DISTRIBUTION/AVAILABILITY STATEMENT
DISTRIBUTION STATEMENT A. Approved for public release: distribution is unlimited.

PA Case Number: 88ABW-2019-4017; Clearance Date: 19 Aug 2019. This document contains color. Journal article published in Materials & Design, Vol. 186, online 7 Nov 2019, published 1 Jan 2020. © Open Access. The U.S. Government is joint author of the work and has the right to use, modify, reproduce, release, perform, display, or disclose the work.
The final publication is available at https://doi.org/10.1016/j.matdes.2019.108316

14. ABSTRACT ***(Maximum 200 words)***
Shape-changing aerospace structures explore the trade-offs between structural performance and efficiency. Herein, a morphing cylinder is optimized to minimize both its work to actuate in bending as well as structural deviations from a prescribed shape. Based on derived linear elastic mechanics of a cylindrical shell in bending, it was determined that favorable designs have high radial stiffness and low axial stiffness. Since no single material can satisfy strain and stiffness constraints, we investigate novel ringed composites composed of both rigid and elastomeric materials. Several distinct archetypal designs were evaluated via finite element analyses to predict the bending kinematics and structural responses of each. Additively manufactured cylinders were fabricated to corroborate these predictions. Digital image correlation was used during bending tests to generate strain contour plots of prototype surfaces. Strong agreement between model predictions and experimental measurements was observed. By systematically varying the dimensions of each archetype via finite element parametric studies, a set of non-dominated designs that satisfy all design criteria was generated. It was determined that flexible skins reinforced with embedded rings were optimal at low (8-15 N·m) and high (>250 N·m) values for the work to articulate and flexible skins reinforced with helical springs were optimal at moderate values (15-250 N·m).

15. SUBJECT TERMS :
Morphing structures, Digital image correlation, Finite element analysis, Kinematic design

16. SECURITY CLASSIFICATION OF:			17. LIMITATION OF ABSTRACT:	18. NUMBER OF PAGES	19a. NAME OF RESPONSIBLE PERSON (Monitor)
a. REPORT	b. ABSTRACT	c. THIS PAGE			Hilmar Koerner
Unclassified	Unclassified	Unclassified	SAR	11	19b. TELEPHONE NUMBER *(Include Area Code)* (937) 255-9324

REPORT DOCUMENTATION PAGE Cont'd

6. AUTHOR(S)

Jeffery W. Baur - AFRL/RXCC

Wesley A. Chapkin, David Ryan Seifert, Maria R. Ward Rashidi - United Technology Corporation

Patrick P. Walgren and Darren J. Hartle - Texas A&M University

Geoffrey J. Frank - University of Dayton Research Institute

7. PERFORMING ORGANIZATION NAME(S) AND ADDRESS(ES)

AFRL/RX
2941 Hobson Way
Wright-Patterson AFB OH 45433

Universal Technology Corporation
1270 N. Fairfield Road
Beavercreek OH 45432-2636

Texas A&M University
Department of Aerospace Engineering
3141 TAMU
College Station TX 77843-3141

University of Dayton Research Institute
300 College Park
Dayton OH 45469-0110

Materials and Design 186 (2020) 108316

Contents lists available at ScienceDirect

Materials and Design

journal homepage: www.elsevier.com/locate/matdes

Bending mechanics of cylindrical skins for morphing aerospace applications

Wesley A. Chapkin [a,b], Patrick Walgren [a,c], Geoffrey J. Frank [a,d], David Ryan Seifert [a,b], Maria R. Ward Rashidi [a,b], Darren J. Hartl [c], Jeffery W. Baur [a,*]

[a] Air Force Research Laboratory, Materials and Manufacturing Directorate, 2941 Hobson Way, WPAFB, OH, 45433-7131, USA
[b] Universal Technology Corporation, 1270 N. Fairfield Road, Beavercreek, OH, 45432-2636, USA
[c] Texas A&M University, Department of Aerospace Engineering, 3141 TAMU, College Station, TX, 77843-3141, USA
[d] University of Dayton Research Institute, 300 College Park, Dayton, OH, 45469-0110, USA

HIGHLIGHTS

- Morphing aircraft design principles were applied to reinforced cylindrical shells in bending.
- Large-diameter cylindrical composites capable of large-scale bending sans buckling were designed, modeled, and fabricated.
- Finite element parametric studies analyzed actuation work and shape deviation resulting in a set of nondominated designs.

GRAPHICAL ABSTRACT

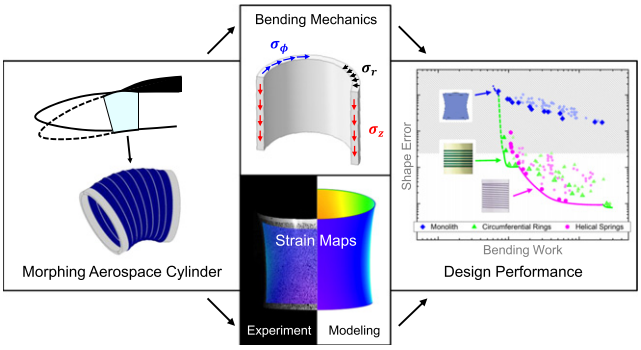

ARTICLE INFO

Article history:
Received 26 September 2019
Received in revised form 25 October 2019
Accepted 27 October 2019
Available online 7 November 2019

Keywords:
Morphing structures
Digital image correlation
Finite element analysis
Kinematic design

ABSTRACT

Shape-changing aerospace structures explore the trade-offs between aerodynamic performance and actuation efficiency. Herein, a morphing cylinder is optimized to minimize both its work to actuate in bending as well as radial deviations. Based on derived linear elastic mechanics of a cylindrical shell in bending, it was determined that favorable designs have high circumferential and low axial stiffnesses. We investigate circumferentially reinforced composites that limit radial displacement and allow for out-of-plane bending. Designs of flexible skins with embedded or underlying reinforcement were modeled, fabricated, and compared to unreinforced skins. Finite element analyses predicted the bending kinematics and structural responses. Digital image correlation used during the bending of physical prototypes generated strain contour plots of cylinder surfaces. Strong agreement between model predictions and experimental measurements was observed. The dimensions of each archetype were systematically varied via finite element modeling to obtain a set of nondominated designs capable of 25° of bending without buckling or large radial displacements. For the examined designs, it was determined that flexible skins reinforced with embedded rings were optimal at low (8–15 N·m) and high (>250 N·m) values for the work to articulate while flexible skins reinforced with underlying helical springs were optimal at moderate values (15–250 N·m).

Published by Elsevier Ltd. This is an open access article under the CC BY-NC-ND license (http://creativecommons.org/licenses/by-nc-nd/4.0/).

* Corresponding author.
E-mail address: jeffery.baur@us.af.mil (J.W. Baur).

https://doi.org/10.1016/j.matdes.2019.108316
0264-1275/Published by Elsevier Ltd. This is an open access article under the CC BY-NC-ND license (http://creativecommons.org/licenses/by-nc-nd/4.0/).

Distribution Statement A. Approved for public release (PA): distribution is unlimited.

1. Introduction

Morphing structures for aerospace applications explore the trade-offs between the complexity, cost, weight, and energy needed to activate a shape-changing system with the anticipated benefits in vehicle agility and range. Morphing skins are important components of these systems. Their primary functions are to accommodate the structural shape change while maintaining a desirable outer mold line with sufficient structural integrity to withstand aerodynamic loads. Depending on the application, successful shape-changing skin designs can exhibit directional and/or temporal differences in stiffness [1]. Stiffness can be engineered to provide the appropriate rigidity in the desired direction to minimize unwanted structural deviations under aerodynamic loading [2,3]. Compliance in a different direction at a specific time can minimize the total actuation energy needed to effect the shape change. The integration of these aspects into a single structure, with the appropriate design and materials, is a key challenge to the effective function of a morphing skin.

A successful design also depends significantly on the type of shape change required for the intended application. Drawing inspiration from nature, morphing wings are the most widely demonstrated example [4,5]. However, as aerospace structures evolve in complexity, other less investigated geometries also warrant examination. One such example includes aerospace structures with ellipsoidal cross-sections such as aircraft fuselages [6,7], satellite struts [8,9], or boom shafts [10,11]. Applying axial bending to this geometry results in an underexplored shape-changing aerospace structure: a morphing cylinder (Fig. 1). A basic requisite for a morphing cylinder considered here is the ability to pivot about a defined point with omnidirectionally radial symmetry. Additionally, the structure must maintain a smooth outer mold line (OML) and exhibit sufficiently high circumferential stiffness to prevent significant radial displacement from aerodynamic loads. The use of low stiffness, high-strain materials and structures in the bending direction ensures the actuation energy required to articulate the cylinder is minimized.

Although the work to actuate and the shape requirements are usually antithetical, one potential solution to avoid sacrificing the performance of one of the objectives is to utilize variable stiffness materials. Compendia of variable stiffness techniques relevant to aerospace structures have been compiled by Kuder et al. [12] and Sun et al. [13] but are limited mainly to airfoils. The approach to deform cylinders in bending using variable stiffness materials has instead been studied more rigorously for medical [14–16] (viz., endoscopes) and soft robotics [17,18] (viz., joints) applications. However, since variable stiffness approaches can increase the required energy to actuate the cylinder, the scope of the current study is limited to solutions with components of constant stiffness. Nevertheless, such structures could readily integrate variable stiffness materials at a later time.

The simplest example is a cylindrical shell composed of a high-strain, high-modulus elastomer. However, single-material solutions are generally infeasible for morphing applications [1]. The maximum strains of higher modulus materials are typically exceeded in many morphing designs. Moreover, materials capable of higher elastic strains generally lack the stiffnesses necessary to maintain an ideal aerodynamic shape under dynamic loading and/or bending. It therefore follows that—similar to past morphing wing designs—a hybrid solution composed of synergistic elements of rigid and high-strain materials is required. These designs combine flexible outer skins that maintain a smooth, continuous outer surface with compliant, load-bearing skeletal structures that reinforce the skins [4]. With this approach, flexible areas reduce the work to actuate to high strains while underlying, overlapping, or embedded rigid layers carry the majority of the structural loads. For example, Park et al. designed and demonstrated a dual-stiffness structure inspired by the skin of an armadillo [19]. By combining stiff and flexible segments, the authors were able to fabricate a prototype capable of switching between rigid and compliant states through sliding and folding mechanisms.

From a design optimization perspective, we seek solutions that *minimize the actuation energy* involved in articulation while concurrently *minimizing the radial shape displacement* of the morphing cylinder. Leveraging results from finite element (FE) parametric studies [20,21], a variety of reinforced designs are considered, and the performance of each is quantified according to these parameters. Prototypes of the top performing designs were fabricated and physically tested to corroborate FE simulations. Using digital image correlation (DIC), strain maps were generated from bending tests to compare with the models.

2. Materials and methods

2.1. Finite element analysis (FEA)

FE models of the different morphing cylinder designs were constructed and analyzed in Abaqus (v6.14, Dessault Systemes Simulia Corp.). The helical spring-reinforced elastomer was analyzed using Abaqus/Explicit. Six separate parts were modeled—an elastomeric outer skin, a helical spring, two clamping bands, and two test frame rings at the top and base. The six elements defined the overall morphing skin system. The analysis used an explicit solution to articulate the assembly. Kinetic energy remained sufficiently low compared to strain energy to provide a quasi-static solution. All parts were modeled with first-order elements using sufficient mesh refinement to adequately resolve strain distributions resulting from bending in each part. A minimum of five elements were used

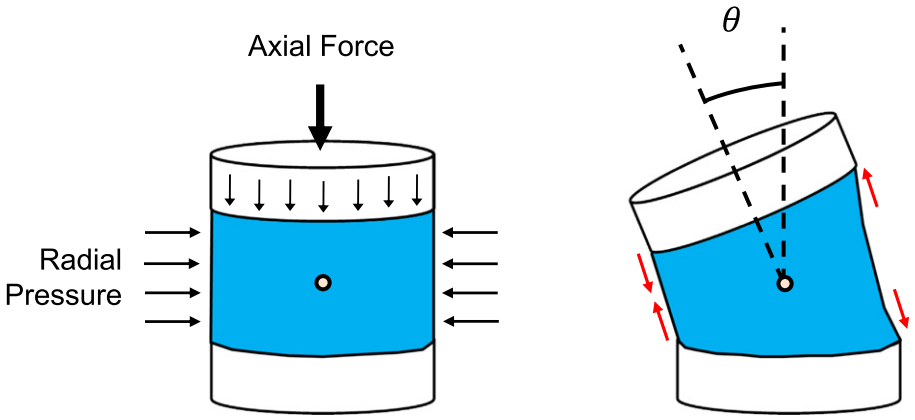

Fig. 1. Schematic of a morphing cylinder with representational aerodynamic forces (left) acting on the (blue) bending region. The bending region undergoes simultaneous tension and compression (right) during articulation as indicated by the red arrows. (For interpretation of the references to color in this figure legend, the reader is referred to the Web version of this article.)

Distribution Statement A. Approved for public release (PA): distribution is unlimited.

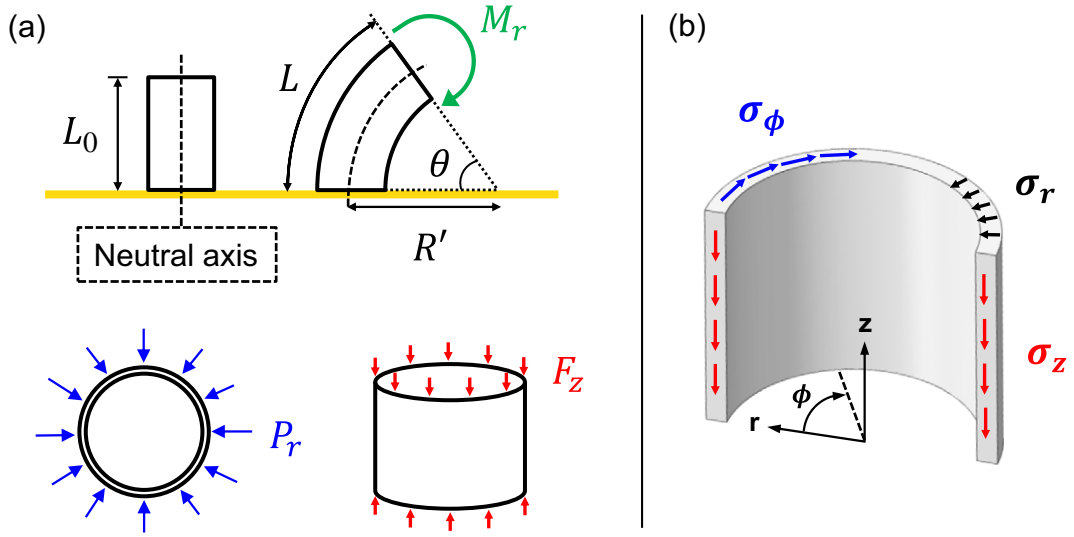

Fig. 2. (a) Large-scale deformation from bending a cylindrical shell with an imposed moment M_r while maintaining shape against an axial load F_z and radial pressure P_r. (b) The applied external forces result in radial, hoop, and axial stresses (σ_r, σ_ϕ, σ_z) in the shell wall.

through the thickness of the steel spring. A minimum of ten elements across each buckling mode were used for the elastomer skin. The elastomeric outer skins were modeled as continuum shells, the steel clamping bands were modeled with standard shells, and the steel spring and aluminum test frame rings were modeled with hexahedral elements. The elastomeric skin was modeled as a hyperelastic material and all metallic parts were modeled as linear elastic. Metallic parts did not exceed material yield stresses, thereby justifying the assumption of elastic behavior. A coefficient of friction of 0.5 was assumed between the spring and elastomer [22]. Each test frame ring was coupled to a reference node for which motion was prescribed to control the articulation of the system. Shape deviation was computed by subjecting cylinder unit cells to a radial pressure (P_r) differential of 20 psi (~138 kPa) and calculating the distance for a certain number of nodes relative to the initial cylindrical configuration (Δr).

2.2. Physical testing

2.2.1. Materials

Polydimethylsiloxane (PDMS) sheets (1 mm in thickness) were purchased from Rubber-Cal Inc. (Santa Ana, CA) and used for the elastomeric skins. Cut sheets were secured to the test fixture with hose clamps. For the reinforced designs, steel helical springs were acquired (Michigan Steel Spring Company, Detroit, MI). All springs had an inside diameter of 17.8 cm. The PDMS sheets were bonded to the springs with Flexseal Black RTV Silicone Sealant from Lawson Inc. (Des Plaines, IL). The springs were then bolted to the fixture for mechanical testing. Information related to the 3D printing of the embedded, reinforcing ring design has been previously published [21].

2.2.2. Mechanical test frame

A custom test fixture was assembled to mechanically test the morphing skin prototype assemblies (Fig. S1(a)). It was designed with the capability of bending a cylinder with a 17.8-cm inside diameter about a central pivot point to a prescribed angle. Articulation kinematics and the resulting strains involved for the studied ranges of motion were collected for various designs.

2.3. Digital image correlation

Elastomeric skins were speckled with a black, latex-based paint. Speckle size and density were tailored to the desired resolution and field of view (Fig. S1(b)). Two cameras (GRAS-20S4M from FLIR Systems, Inc.) with 35 mm lenses (Xenoplan 1.4/17–0903 from Schneider Kreuznach) were placed 0.75 m from the mounted skins. The strain maps from digital image correlation were generated with VIC-3D software from Correlated Solutions [23].

3. Results

3.1. Linear elastic mechanics of a bending cylinder

Whereas morphing wings have received growing interest from the aerospace community, other geometric configurations have remained relatively unexplored for aerospace purposes. Herein, we investigate one such geometry—a large-diameter cylindrical shell in bending (Fig. 2).

A morphing cylinder should articulate to a prescribed angle θ under certain axial (F_z) and radial (P_r) loads (Fig. 2(a)) without exceeding critical stresses (σ_{crit}) or strains (ε_y) that lead to buckling of the structure or yield in the material. For a monolithic cylinder subjected to a bending moment about its radial axis, the stress/strain relationship can be defined according to

$$\begin{bmatrix}\varepsilon_r\\ \varepsilon_\phi\\ \varepsilon_z\end{bmatrix} = \begin{bmatrix}\frac{1}{E_r} & -\frac{\nu_{\phi r}}{E_\phi} & -\frac{\nu_{zr}}{E_z}\\ -\frac{\nu_{r\phi}}{E_r} & \frac{1}{E_\phi} & -\frac{\nu_{z\phi}}{E_z}\\ -\frac{\nu_{rz}}{E_r} & -\frac{\nu_{\phi z}}{E_\phi} & \frac{1}{E_z}\end{bmatrix}\begin{bmatrix}\sigma_r\\ \sigma_\phi\\ \sigma_z\end{bmatrix} \quad (1)$$

where ε is strain, E is Young's modulus, ν is Poisson's ratio, σ is stress, and the (r, ϕ, z) subscripts denote radial, hoop (or circumferential), and axial directions, respectively (Fig. 2(b)). To comply with the imposed buckling constraint, $\sigma<\sigma_{crit}$ must hold for the compression side of the cylinder. On the tension side, the yield criterion $\varepsilon<\varepsilon_y$ must be satisfied. For a cylindrical shell in bending, the dominant stress and strain terms are in the axial direction (Fig. S2) where

$$\varepsilon_z = -\frac{\nu_{rz}}{E_r}\sigma_r - \frac{\nu_{\phi z}}{E_\phi}\sigma_\phi + \frac{1}{E_z}\sigma_z \,. \quad (2)$$

For thin cylindrical shells (inner shell radius to thickness ratio of $r_i/t \geq 10$) under uniformly distributed loading, σ_r is negligibly small [24]. Reworking Eq. (2) into an expression for the axial stress σ_z from bending and pressure becomes

$$\sigma_z \approx \varepsilon_z^{bend} E_z + \frac{E_z}{E_\phi}\nu_{\phi z}\sigma_\phi \,. \quad (3)$$

Including a term for the axial stress due to the applied force F_z results in

$$\sigma_z \approx \varepsilon_z^{bend} E_z + \frac{E_z}{E_\phi}\nu_{\phi z}\sigma_\phi + \frac{F_z}{\pi t(2r_i + t)} \,, \quad (4)$$

which shows contributions to the axial stress from bending, radial pressure, and the axial loading, respectively.

As shown in Fig. 2(a), the length of the neutral axis L_0 can be related to the radius of curvature R' by $L_0 = \theta R'$. At the outer wall of the cylinder, the length of the side in tension is $L = \theta(R' + r_o)$ where r_o is the outer wall radius. The axial strain from bending ($\varepsilon_z^{bend} = \Delta L/L_0$) therefore becomes

$$\varepsilon_z^{bend} = \frac{\theta(R' + r_o) - \theta R'}{\theta R'} \,, \quad (5)$$

which simplifies to

$$\varepsilon_z^{bend} \approx \frac{r_o\theta}{L_0} \,. \quad (6)$$

Distribution Statement A. Approved for public release (PA): distribution is unlimited.

The axial bending strain in Eq. (6) coupled with the hoop stress arising from uniform radial pressure ($\sigma_\phi \approx P_r r_o/t$) [24] can be substituted into Eq. (4) to yield

$$\sigma_z \approx E_z r_o\left(\frac{\theta}{L_0}+\frac{P_r \nu_{\phi z}}{E_\phi t}\right)+\frac{F_z}{\pi t(2r_i+t)} . \tag{7}$$

Since axial stresses from bending dominate the other terms for most external, aerospace loading cases (Fig. S2), Eq. (7) simplifies to

$$\sigma_z \approx E_z \frac{r_o\theta}{L_0} . \tag{8}$$

Even though an initial, non-axisymmetric stress distribution and ovalization of the cross-section complicate analyses of the compressive stresses that arise from bending, the buckling resistance for a cylinder in bending is essentially equivalent to that for a cylinder subjected to uniform axial compression [25]. Because of this, σ_z can be compared to a well-established critical stress for elastic buckling of thin-shell cylinders [26,27]:

$$\sigma_{crit} \approx \frac{E_z}{\sqrt{3(1-\nu^2)}}\psi\frac{t}{\bar{r}} \tag{9}$$

where $\bar{r}$ is the mean shell radius and ψ is a knockdown factor dependent on aspect ratio and material anisotropy that typically falls between 0.2 [28] and 0.65 [29]. Equating Eqs. (8) and (9) demonstrates that for a displacement-prescribed case, buckling is modulus-independent and determined mainly by geometry. The angle at which buckling occurs is roughly

$$\theta_{crit} \approx \frac{\psi L_0 t}{r_o \bar{r}\sqrt{3(1-\nu^2)}} . \tag{10}$$

The effects of varying a monolithic cylinder's geometry on θ_{crit} are captured in Fig. 3. For a set $t/\bar{r}$, θ_{crit} scales with aspect ratio L_0/r_o ($t/\bar{r} = 0.1$ in Fig. 3a). For the dimensions studied herein, buckling as defined in Eq. (10) occurs around 4° of bending for a monolithic cylindrical shell. Either decreasing the shell's radius or increasing its length will increase the critical buckling angle of a structure. However, if a cylindrical shell's length, radius, and thickness are allowed to vary freely, θ_{crit} exists as a curved surface in $t-r_o-L_0$ space (Fig. 3b). In general, high-aspect ratio cylinders with thick walls result in structures capable of higher bending angles without buckling.

Morphing aerospace structures are typically designed to minimize the energy requirements for shape change, which can be accomplished by reducing the flexural rigidity of the structure. The maximum allowable bending stiffness of a design is limited solely by the output of the actuator(s) used. The viability of a morphing cylinder design can therefore be assessed via the work to articulate, which can be calculated for a specified bending angle according to

$$W(\theta) = \int_0^\theta M_r d\theta \tag{11}$$

where the moment about its radial axis is

$$M_r = \frac{E_z I}{L_0}\theta, \tag{12}$$

and I is the second moment of area. For a thin-shell cylinder [30], this results in

$$W = \frac{E_z\theta^2}{L_0}\frac{\pi}{8}\left(r_o^4-r_i^4\right) . \tag{13}$$

Reducing flexural rigidity (EI) for the purposes of minimizing the work to actuate can, however, have the antagonistic effect of decreasing the structure's ability to resist buckling under compressive axial forces and radial pressure gradients. Buckling is typically detrimental (when not engineered to occur) because it can result in a decrease in supported loads, local plasticity in the material, and out-of-plane deformations that increase drag. In addition to compressive loads, pressure gradients observed by the morphing cylinder require a certain radial stiffness to maintain an aerodynamically favorable OML. Axial and radial deviations can be expressed as the sum of the contributions to OML displacement from F_z and P_r according to [24]

$$\Delta L = \Delta L_{F_z} + \Delta L_{P_r} = -\frac{F_z}{E_z t}+\frac{P_r r_o \nu_{rz} L_0}{E_\phi t} \tag{14}$$

$$\Delta r = \Delta r_{F_z} + \Delta r_{P_r} = \frac{F_z \nu_{zr} r_o}{L_0 E_z t}-\frac{P_r r_o^2}{E_\phi t} . \tag{15}$$

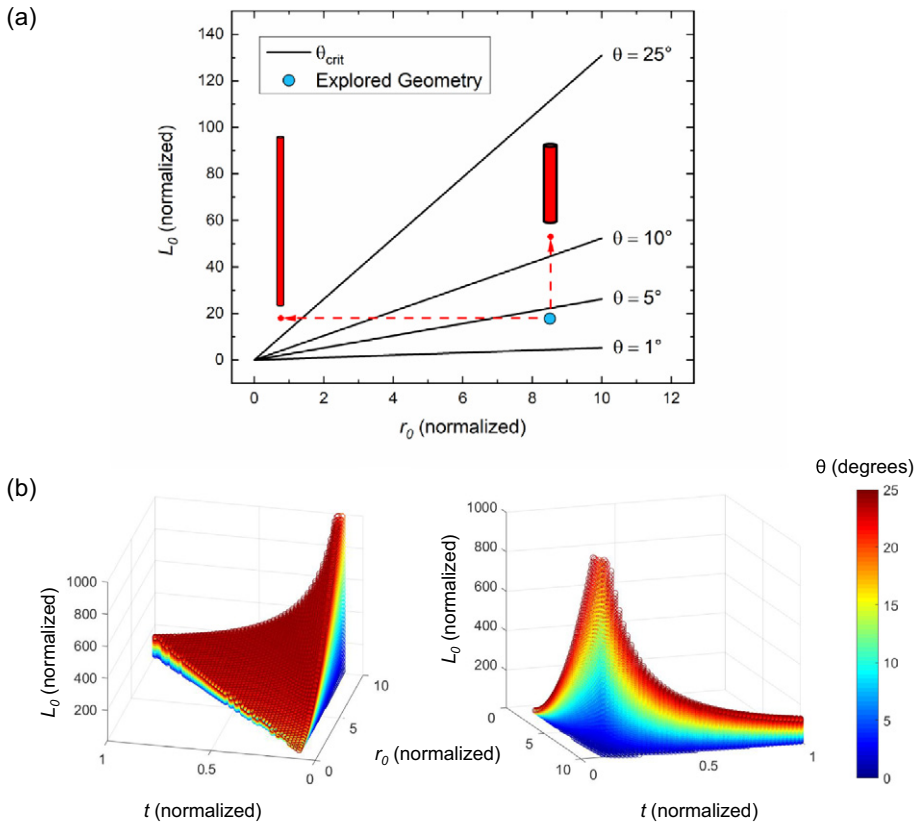

Fig. 3. Critical buckling angles, θ_{crit}, as a function of a monolithic cylindrical shell's geometry. (a) For a defined thickness to radius ratio of $t/\bar{r} = 0.1$, θ_{crit} varies linearly with the cylindrical shell's aspect ratio, L_0/r_o. b) θ_{crit} is shown as a function of freely varying t, r_o, and L_0. Constants ν and ψ both equal 0.5 in (a) and (b).

Distribution Statement A. Approved for public release (PA): distribution is unlimited.

Reworking Eqs. (14) and (15) to show global strains in the structure yields

$$\varepsilon_L = \frac{\Delta L}{L_0} = -\frac{A}{E_z} + \frac{B\nu_{rz}}{E_\phi} \tag{16}$$

$$\varepsilon_r = \frac{\Delta r}{r_o} = \frac{A\nu_{zr}}{E_z} - \frac{B}{E_\phi} \tag{17}$$

where axial and radial terms are respectively grouped together as $A = F_z/(L_0 t)$ and $B = P_r r_o/t$. From the relationships laid out in Eqs. (13), (16) and (17), it becomes apparent that changes in a monolithic cylinder's modulus or thickness will have an antagonistic effect on the objectives to minimize both actuation work (min E_z, t) and deviations from a prescribed shape (max E_z, E_ϕ, t).

For a positive effective Poisson's ratio of the cylinder, deformation arising from compressive axial forces and radial pressures occurs in opposite directions. By tailoring E_z and E_ϕ, a cylindrical shell can counteract the external forces for a given load environment. Consequently, an anisotropic material could conceivably assume an isostatic equilibrium. Although the zero-strain cases in the axial and radial directions defined in Eqs. (16) and (17) do not overlap for most geometries and load environments, combinations of acceptably low radial and axial strains would exist at high values of E_z and E_ϕ.

In addition to minimizing deviations from a precise shape, morphing aerospace structures are limited by energy costs of changing shape. Since a stiffer structure requires a larger amount of actuation energy to articulate, the composition of the bendable region is actuator-dependent and restricted to lower axial moduli. This low stiffness requirement eliminates most commonly used structural materials (e.g. lightweight metals and fiber-reinforced composites). Nonetheless, certain lower-modulus, anisotropic configurations (e.g. reinforced elastomers) could still exist for acceptably low deformations in the cylinder. The crucial disadvantage of precisely tailoring E_z and E_ϕ to a specific static environment is that small changes in the loading conditions would perturb any balance of forces, effectively making this strategy incompatible with a dynamic system. This finding, in conjunction with contrasting work/shape objectives and geometrically driven buckling of thin-shell cylinders, therefore requires the exploration of more complex, structured composites with corresponding nonlinear models.

3.2. Design metrics

Design objectives for the morphing cylinder include minimizing both the actuation energy to bend the cylinder, Eq. (11), as well as its deviation from a prescribed shape under loading. Ideally, a desired aerodynamic profile should be maintained when the structure is both unloaded and fully loaded. It is therefore critical that a viable skin design demonstrates sufficient out-of-plane stiffness to withstand aerodynamic loading as well as precise shape control. To this end, a shape error parameter is used to quantify deviation from the unperturbed dimensions under a pressure load. Several metrics were evaluated, and a root mean square error (ε_{RMS}) value was determined to be the most appropriate [20]. As a result, the quality of a surface profile for each design under nominal pressurization was assessed according to

$$\varepsilon_{RMS} = \sqrt{\frac{\sum_{i=1}^{N} \varepsilon^2}{N}} \tag{18}$$

where $\varepsilon = |(x_i - \hat{x}_i), (y_i - \hat{y}_i), (z_i - \hat{z}_i)|$ for N number of nodes in a part compared to an unarticulated, reference $(\hat{x}, \hat{y}, \hat{z})$ configuration (Fig. S3).

In addition to minimizing the two design objectives, several constraints are applied. Cylinders are required to elastically articulate to at least 25° in all directions (i.e. $\theta_{max} \geq 25°$) without buckling. Thus, stresses in the materials should not exceed critical buckling values for the structure (i.e. $\sigma < \sigma_{crit}$), and local strains should not exceed yield strains of the materials (i.e. $\varepsilon < \varepsilon_y$). While the design objective for maintaining a precise shape is to minimize ε_{RMS}, an added constraint is that no part of the outer surface deviates more than 1.25 mm from its original shape when placed under nominal loading (i.e. $\Delta r \leq 1.25$ mm). Free variables include the cylinder's composition and shape of any substructures. A list of design objectives, constraints, and free variables is summarized in Table 1.

3.3. Morphing cylinder designs

As shown by Eqs. (13)–(15), the top performing morphing cylinder designs demonstrate both axial compliance and radial rigidity. While monolithic solutions are inherently limited, the inclusion of reinforcing substructures opens a wealth of design space. To increase the radial stiffness of a cylinder with minimal changes to its axial stiffness, reinforcing circumferential rings can be incorporated [21]. This concept leads to several different design classes in which reinforcing skeletons provide structural support for flexible outer skins. Elastomeric skins with both embedded and subcutaneous reinforcing elements are considered.

Physical prototypes and their corresponding FE models for several bending cylindrical shells are presented in Fig. 4. In addition to a baseline monolithic elastomeric cylinder, these include (1) a bio-inspired [21], compliant composite with rigid support material embedded in a flexible matrix and (2) an elastomeric outer skin with an underlying helical spring. The incorporation of reinforcement with a flexible skin has two requirements—it provides increased radial stiffness without hindering the range of motion in bending and greatly increasing the work needed to articulate. One such composite structure is a two-phase system with alternating rigid and compliant ringed sections. Based on their positions and dimensions, the rigid segments can give the cylinder a preferential deformation axis. Anisotropy in the structure can therefore be leveraged to selectively stiffen the cylinder in load-bearing directions. A reinforcing spring works in a similar manner—it enhances the radial rigidity of the skin and can be parameterized to allow for a flexible structure in bending. Flexible hosing is an archetypal example of this design.

3.4. Mechanical testing of prototypes

Articulation kinematics of the designs were studied experimentally in order to compare with FE models. Prototypes of the designs in Fig. 4 were created and tested using a custom-made test fixture that allowed cylindrical shells to be placed in bending. DIC was employed during testing to track the evolution of strain profiles in the deformed structures.

3.4.1. Monolithic elastomer

Results for the baseline elastomeric skin (with no reinforcement) are shown in Fig. 5. The skin is pretensioned to 30% strain to avoid immediate compressive buckling upon bending. Strain maps were generated as a function of articulation angle up to 25° at which point the structure buckled. Logarithmic strain (LE) values computed with DIC were in good agreement with those predicted by FEA for both the tension and compression sides of the cylinder.

3.4.2. Laminated helical springs

Skin assemblies reinforced by helical springs were tested, and the results are collected in Fig. 6. Helices were unbonded along the length of the skins and rigidly clamped at the ends. Individual coils were thus free to slide relative to the skin, a mechanism that can be difficult to capture in FEA. Modeled strain maps closely approximate experimental values with local maxima at the top and base of the structure in good agreement. Small decreases in strain predicted near the reinforcing coils were not resolved using DIC. On the compression side of the cylinder, ridges corresponding to the reinforcing coils were observed and prevented global buckling up to 10° of articulation (Fig. S4). A 20% pre-strain case was also tested, which showed buckling around 25° that was consistent with the FEA (Fig. S5).

3.4.3. Embedded circumferential rings

Articulation data for the embedded, reinforcing ring design are collected in Fig. 7. Strain profiles generated from DIC data are compared to those predicted in FEA for articulation angles of 10° and 20° on the tension side of the cylinder. Although sharp discontinuities in strain are not resolved in DIC, the periodicity of high- and low-strain regions matches the FEA. These regions correspond to the flexible elastomer and rigid reinforcing rings, respectively. On the compression side, the incompressible elastomer ($\upsilon = 0.5$) visibly bulges outward. The ridges formed from the bulging elastomer are similar to those predicted in the FE models. Additional information pertaining to the physical testing and FE modeling of this design can be found elsewhere [21].

Table 1
Constraints, objectives, and free variables for a morphing cylinder. Metrics are defined for each, and analytical derivations for monolithic cylindrical shells are also included.

	Functions	Metrics	For a monolithic cylindrical shell
Objectives	Minimizes bending work	$W(\theta) = \int_0^\theta M_r d\theta$	$W = \frac{E_z \theta^2}{L_0}\frac{\pi}{4}(r_o^4 - r_i^4)$
	Minimizes structural deviations	$\varepsilon_{RMS} = \sqrt{\frac{\sum_{i=1}^{N}\varepsilon^2}{N}}$	$\Delta L = \Delta L_{F_z} + \Delta L_{P_r} = -\frac{F_{z0}}{E_z t} + \frac{P_r r_o \nu_{rz} L_0}{E_\phi t}$ $\Delta r = \Delta r_{F_z} + \Delta r_{P_r} = \frac{F_z \nu_{zr} r_o}{L_0 E_z t} - \frac{P_r r_o^2}{E_\phi t}$
Constraints	Avoids buckling of the structure	$\sigma < \sigma_{crit}$	$\theta < \frac{\psi L_0 t}{r_o \bar{r}\sqrt{3(1-\nu^2)}}$
	Avoids yielding of the material(s)	$\varepsilon < \varepsilon_y$	$\frac{r_o \theta}{L_0} < \varepsilon_y$
	Does not exceed 1.25 mm at any point from ideal shape under loading	$\lvert\Delta r\rvert < 1.25$ mm	
Free Variables	Material composition, substructure dimensions		

Distribution Statement A. Approved for public release (PA): distribution is unlimited.

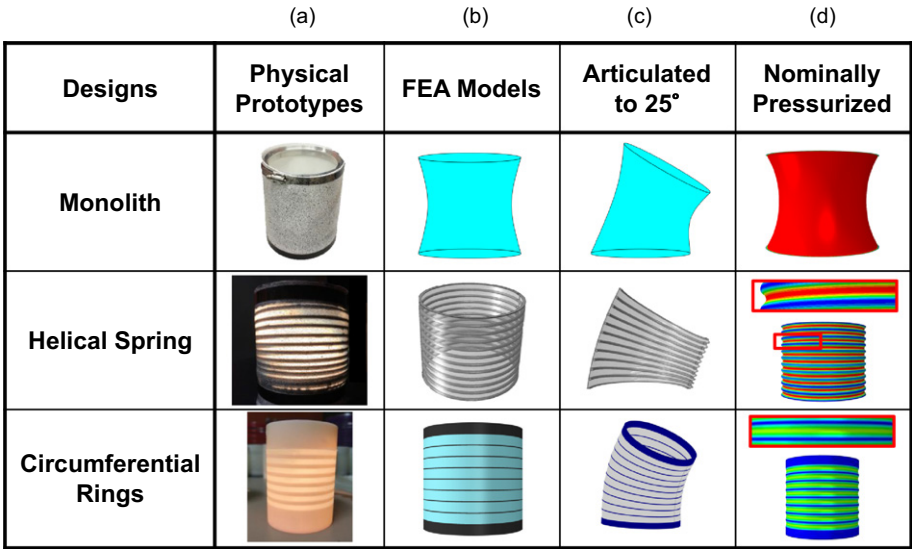

Fig. 4. Archetypal examples of each studied design in the forms of (a) physical prototypes and FE models shown (b) statically, (c) in bending, and (d) nominally pressurized. Parts of each archetype in (d) for which $|\Delta r|$ exceeds 1.25 mm are colored red. (For interpretation of the references to color in this figure legend, the reader is referred to the Web version of this article.)

3.5. Design space exploration

Since mechanical testing of archetypal prototypes experimentally corroborated the kinematics of the FE models, FEA could then be used to reliably quantify the relevance of each class of designs shown in Fig. 4. This was achieved via the two previously defined metrics in Eqs. (11) and (18): the work to articulate, $W(\theta)$, and the quality of the surface profile determined from an RMS error value, ε_{RMS}. FE parametric studies and topology optimization were used to conceptualize specific morphologies for composite cylinders. Composite designs were limited to two materials with a large difference in modulus ($E_{rigid}/E_{compliant}$~10^3). Analyses considered full (25°) articulation, radial pressure, and yield criteria to simulate the complex loading environment of the morphing cylinder. This approach yielded archetypes displaying horizontal rings, corroborating the selection of the aforementioned bio-inspired designs. Additional information pertaining to the optimization of the bio-inspired composites can be found elsewhere [21].

FE parametric studies generated performance data for the design space of each investigated class of structures (Fig. 8). For each type of cylinder, structural and material design parameters were varied (e.g. elastomer pre-strain, elastomer thickness, and the number and dimensions of reinforcing elements). The work to articulate was computed for the monolith as well as the skin/skeleton ensemble for helical spring and embedded rings designs. A front of nondominated designs for the chosen performance trade-offs (actuation work vs. structural deviation) was created from the entire design space of the three studied classes of cylinders. Regions of the design space where surface roughness would exceed a nominal tolerance are shaded; a $|\Delta r|$ limit of 1.25 mm was used in this study. This eliminates all designs that would either yield or buckle during flight or negatively impact the aerodynamics of the structure past an impermissible point.

As shown in Fig. 8, unreinforced designs fail to satisfy all design requirements; for the monolithic elastomeric skins, deviations from the OML exceeded the ±1.25 mm radial tolerance for all analyzed cases. Reinforcement provided by the helical springs and embedded rings in many cases decreases the radial distortions of the cylinders to acceptable levels. While monolithic elastomers are uncompetitive, the nondominated front for the circumferentially reinforced design space switches between helical spring-reinforced skins and embedded rings, resulting in a mixture of the top-performing designs. The nondominated front consists mostly of designs with non-zero elastomeric pre-strain, suggesting that there is an optimal value that balances the resistance to buckling with the necessary work to articulate.

4. Discussion

Several conclusions can be drawn from the different morphing cylinders investigated herein. While each falls somewhere on a nondominated front of performance (Fig. 8), limitations exist for all tested designs. Monolithic cylindrical shells either bulge or collapse radially under pressure with thin, compliant walls or buckle catastrophically during articulation for thicker, high-durometer elastomers. Since no single material satisfies the contradictory requirements of a morphing cylinder, a composite made of synergistic elements is needed. Helical springs can improve the radial stiffness of the skin without

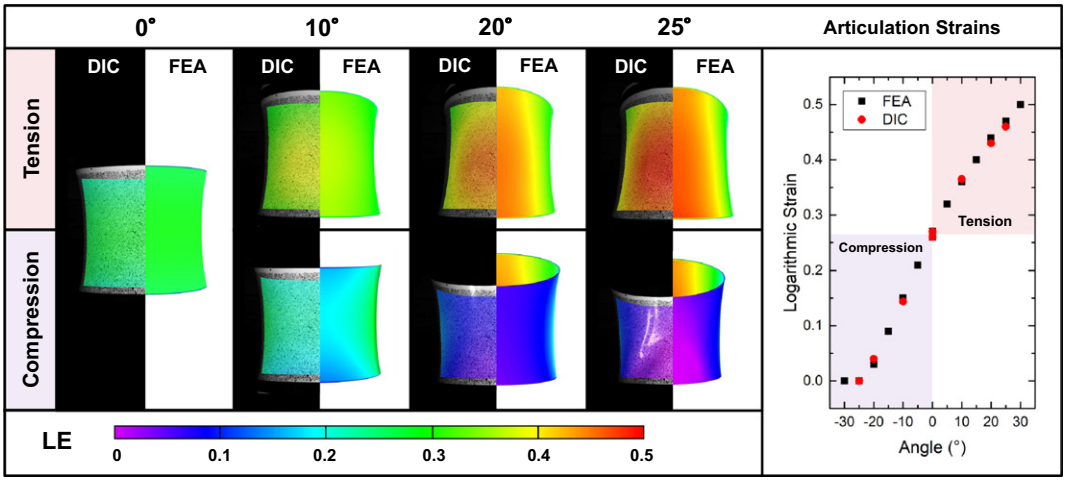

Fig. 5. DIC (black background) and corresponding FE (white background) strain maps for a monolithic elastomeric skin articulating to 25°. Maximum (tension) and minimum (compression) logarithmic strain values are plotted for comparison. The skin is pretensioned 30%. Cylinders are 18 cm in diameter.

Distribution Statement A. Approved for public release (PA): distribution is unlimited.

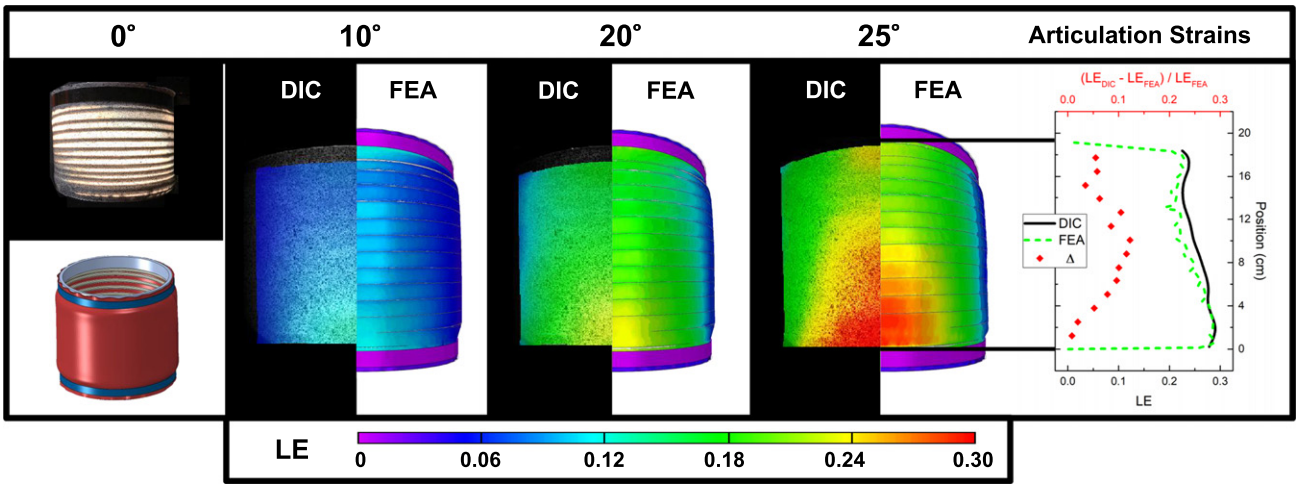

Fig. 6. DIC and corresponding FE strain maps for a helical spring-reinforced elastomeric skin articulating to 25°. Line slices of the strain profiles at 25° of articulation on the tension side are compared graphically. The fractional difference (Δ) between DIC and FEA values is shown at regular intervals. Cylinders are 19 cm in diameter.

greatly increasing the work to articulate. However, low spring constants required to minimize work provide meager improvements in axial stiffness, which cause coils to buckle out of plane in compression. An initial pre-strain placed on the spring/skin ensemble can be used to avoid compression during bending; however, long-term storage, especially at temperatures below the elastomer's glass transition temperature, becomes impractical. The composite cylinders with rigid rings are the best-performing design explored here in terms of minimizing work while meeting shape requirements without buckling. Alternating rings of material act in series and allow compliant sections to undergo a majority of the strain involved in bending. The reinforcing rings prevent buckling of the cylinder (Fig. S6) with minimal effects on actuation. The mechanical performance of this design depends heavily on the interface between the materials and may be a potential drawback in torsion. Additionally, the performance of each archetype is expected to improve with optimization, but the computational complexity of the FE models precluded that study in this work.

5. Conclusions

This work detailed the general mechanics, FE modeling, and characterization of a morphing cylinder for aerospace applications—a shape-changing geometry heretofore limited to the medical fields and soft robotics. From linear elastic mechanics of a cylindrical shell in bending, it was shown that buckling of a monolithic structure is modulus-independent and determined by geometry. Additionally, changes in the cylinder's modulus antagonistically affect the opposing design requirements of minimizing articulation work and shape error. Finally, precisely tailoring anisotropy in a cylinder's stiffness to counteract external forces is incompatible with a dynamic aerospace environment. Consequently, substructured composites are needed to meet morphing cylinder design objectives and satisfy constraints.

Several designs were considered, and finite element parametric studies identified optimized structures for minimizing actuation energy inputs while maintaining desirable shape profiles. Results from finite element analyses were analytically corroborated and experimentally validated via digital image correlation. Based on the imposed metrics, it was determined that two designs occupied the top performing design space: (1) structures with alternating rings of stiff and flexible material and (2) elastomeric skins reinforced with helical springs. At low (8–15 N·m) and high (>250 N·m) values for the work to articulate, flexible skins reinforced with embedded rings were more competitive. At moderate values (15–250 N·m), flexible skins reinforced with helical springs were preferable. As morphing technology advances, the best solutions for meeting both structural and shape-changing requirements will involve both shape optimization of and materials selection for distinct elements that operate synergistically.

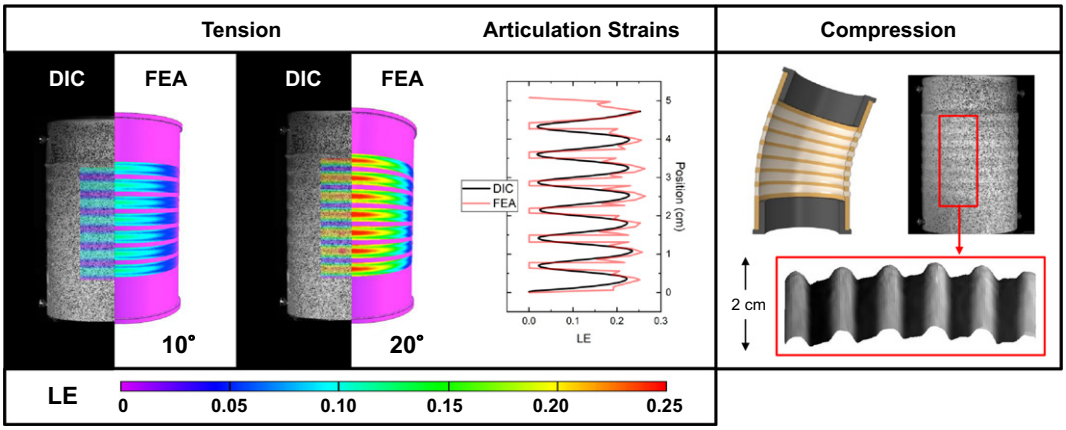

Fig. 7. Tension and compression sides of an embedded circumferential ring-reinforced elastomeric skin places in bending. On the tension side, DIC and corresponding FE strain maps are shown at 10° and 20° articulation. Line slices of the strain profiles on the tension side at 20° of articulation are compared graphically. On the compression side, elastomer bulges are visible at 20° of bending and resemble those predicted by FE models.

Distribution Statement A. Approved for public release (PA): distribution is unlimited.

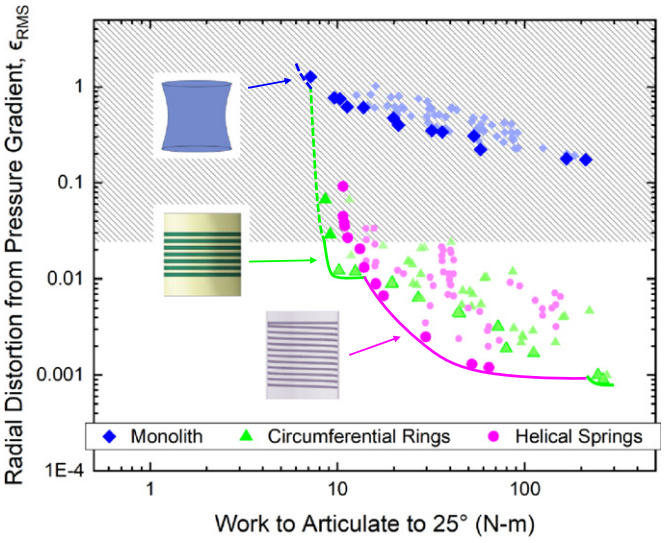

Fig. 8. – FE performance data for the studied designs. The shaded region identifies designs where $|\Delta r| > 1.25$ mm. Nondominated designs, from which a front for work-shape tradeoffs are drawn, are emphasized.

Data availability

The raw/processed data required to reproduce these findings cannot be shared at this time as the data also form part of an ongoing study.

Declarations of interest

None.

CRediT authorship contribution statement

Wesley A. Chapkin: Conceptualization, Data curation, Formal analysis, Investigation, Methodology, Writing - original draft. **Patrick Walgren:** Data curation, Investigation, Writing - review & editing. **Geoffrey J. Frank:** Conceptualization, Data curation, Investigation, Writing - review & editing. **David Ryan Seifert:** Investigation, Writing - review & editing. **Maria R. Ward Rashidi:** Conceptualization, Investigation, Methodology. **Darren J. Hartl:** Supervision. **Jeffery W. Baur:** Conceptualization, Funding acquisition, Methodology, Supervision, Writing - review & editing.

Acknowledgements

Funding for this research was provided through an Air Force Research Lab Commander's Research and Development Fund. The authors also acknowledge contributions by Tal Dohn in the physical testing, Ashley Schrader with finite element models, Mike Pratt for the custom test fixture, and Dan Rapking for helpful conversations concerning digital image correlation.

Appendix A. Supplementary data

Supplementary data to this article can be found online at https://doi.org/10.1016/j.matdes.2019.108316.

References

[1] C. Thill, J. Etches, I. Bond, K. Potter, P. Weaver, Morphing skins, Aeronaut. J. 112 (2008) 117–139, https://doi.org/10.1017/S0001924000002062.
[2] I. Dayyani, M.I. Friswell, Multi-objective optimization for the geometry of trapezoidal corrugated morphing skins, Struct. Multidiscip. Optim. (2017) 331–345, https://doi.org/10.1007/s00158-016-1476-4.
[3] H. Baier, L. Datashvili, Active and morphing aerospace structures–A synthesis between advanced materials, structures and mechanisms, Int'l J. Aeronaut. Sp. Sci. 12 (2011) 225–240, https://doi.org/10.5139/IJASS.2011.12.3.225.
[4] S. Barbarino, O. Bilgen, R.M. Ajaj, M.I. Friswell, D.J. Inman, A review of morphing aircraft, J. Intell. Mater. Syst. Struct. 22 (2011) 823–877, https://doi.org/10.1177/1045389X11414084.
[5] K. Jha, Akhilesh, J.N. Kudva, Morphing aircraft concepts, classifications, and challenges, Proc. SPIE 5388, Smart Struct. Mater. 2004, pp. 213–224, https://doi.org/10.1117/12.544212.
[6] W.E. Goff, Droop Nose, Flight Int. 1971 257–260. https://www.flightglobal.com/pdfarchive/view/1971/1971 - 1503.html.
[7] J. Riemenschneider, M. Radestock, S. Vasista, H.P. Monner, O. Huxdorf, Droop nose with elastic skin, SMASIS2016-9130 Proc. ASME 2016 Conf. Smart Mater. Adapt. Struct. Intell. Syst., 2016https://doi.org/10.1115/SMASIS2016-9130.
[8] D.P. Cadogan, J.K. Lin, M.S. Grahne, The development of inflatable space radar reflectarrays, AIAA-99-1517 40th AIAA/ASME/ASCE/AHS/ASC Struct. Struct. Dyn. Mater. Conf., 1999https://doi.org/10.2514/6.1999-1517.
[9] K.N. Slade, M.L. Tinker, J.O. Lassiter, R. Engberg, Dynamics of an inflatable structure in vacuum and ambient conditions, AIAA J. 39 (2001) 894–901, https://doi.org/10.2514/2.1393.
[10] A.E. Hoyt Haight, L.A. Harrah, R.E. Allred, S. Scarborough, D. Gleeson, D. Cadogan, Thermal reversibility and morphing of light curing inflatable composite booms, AIAA 2005-1808 46th AIAA/ASME/ASCE/AHS/ASC Struct. Struct. Dyn. Mater. Conf., 2005https://doi.org/10.2514/6.2005-1808.
[11] J. Zhang, A. Song, X. Xu, W. Lu, A rigid and flexible structures combined deployable boom for space exploration, 2016 IEEE/RSJ Int. Conf. Intell. Robot. Syst., IEEE 2016, pp. 2920–2926, https://doi.org/10.1109/IROS.2016.7759452.
[12] I.K. Kuder, A.F. Arrieta, W.E. Raither, P. Ermanni, Variable stiffness material and structural concepts for morphing applications, Prog. Aerosp. Sci. 63 (2013) 33–55, https://doi.org/10.1016/j.paerosci.2013.07.001.
[13] J. Sun, Q. Guan, Y. Liu, J. Leng, Morphing aircraft based on smart materials and structures: a state-of-the-art review, J. Intell. Mater. Syst. Struct. 27 (2016) 2289–2312, https://doi.org/10.1177/1045389X16629569.
[14] A. Yagi, K. Matsumiya, T. Dohi, Slider linkage lock mechanism using Air pressure for rigid-flexible outer sheath for endoscopic surgery, 1st Asian Symp. Comput. Aided Surg. - Robot. Image Guid. Surg. 2005, pp. 194–197, https://doi.org/10.5759/jscas1999.7.127.
[15] A.J. Loeve, D.H. Plettenburg, P. Breedveld, J. Dankelman, Endoscope shaft-rigidity control mechanism: "FORGUIDE", IEEE Trans. Biomed. Eng. 2012, pp. 542–551, https://doi.org/10.1109/TBME.2011.2175730.
[16] Y. Kim, S. Cheng, S. Kim, K. Iagnemma, Design of a tubular snake-like manipulator with stiffening capability by layer jamming, IEEE/RSJ Int. Conf. Intell. Robot. Syst. 2012, pp. 4251–4256, https://doi.org/10.1109/IROS.2012.6385574.
[17] O. Tabata, S. Konishi, P. Cusin, Y. Ito, F. Kawai, S. Hirai, et al., Micro fabricated tunable bending stiffness devices, Sens. Actuators 89 (2001) 119–123, https://doi.org/10.1016/S0924-4247(00)00538-0.
[18] F. Connolly, C.J. Walsh, K. Bertoldi, Automatic design of fiber-reinforced soft actuators for trajectory matching, Proc. Natl. Acad. Sci. 114 (2017) 51–56, https://doi.org/10.1073/pnas.1615140114.
[19] Y. Park, J. Lee, S. Jeon, H. Ahn, J. Koh, J. Ryu, et al., Dual-stiffness structures with reconfiguring mechanism: design and investigation, J. Intell. Mater. Syst. Struct. 27 (2016) 995–1010, https://doi.org/10.1177/1045389X15577642.
[20] P.P. Walgren, D.J. Hartl, R. Seifert, W.A. Chapkin, G.J. Frank, J.W. Baur, Efficient design of a smooth bending cylinder via parametric studies and optimization, 27th AIAA/AHS Adapt. Struct. Conf., 2019https://doi.org/10.2514/6.2019-1633.
[21] M.R.W. Rashidi, G.J. Frank, T. Dohn, R. Seifert, W.A. Chapkin, J.W. Baur, Biomimicry of the armadillo carapace for the design of bending cylinders for aerospace applications, 27th AIAA/AHS Adapt. Struct. Conf., 2019https://doi.org/10.2514/6.2019-1632.
[22] Silicone Molding Design Manual. sixth ed., Albright Technologies, Leominster, MA, 2005 11.
[23] Correlated Solutions, VIC-3D V7 Reference Manual, Columbia, SC. 2014.
[24] W.C. Young, Roark's Formulas for Stress and Strain, sixth ed. McGraw-Hill, New York, 1989.
[25] J. Amdahl, Buckling and Ultimate Strength of Marine Structures, TMR4205, (-Chapter 5): Buckling of Cylindrical Shells 2005.
[26] D.O. Brush, B.O. Almroth, Buckling of Bars, Plates and Shells, McGraw-Hill, New York, 1975.
[27] S. Houliara, S.A. Karamanos, Buckling of thin-walled long steel cylinders subjected to bending, J. Press. Vessel Technol. 133 (2011) https://doi.org/10.1115/1.4002902.
[28] J.W. Hutchinson, Knockdown factors for buckling of cylindrical and spherical shells subject to reduced biaxial membrane stress, Int. J. Solids Struct. 47 (2010) 1443–1448, https://doi.org/10.1016/j.ijsolstr.2010.02.009.
[29] J.P. Peterson, P. Seide, V.I. Weingarten, Buckling of Thin-Walled Circular Cylinders, NASA SP-8007 1968.
[30] M.F. Ashby, Materials Selection in Mechanical Design, fourth ed. Elsevier Ltd., Oxford, UK, 2011.

Distribution Statement A. Approved for public release (PA): distribution is unlimited.